

# GRB 080928 afterglow imaging and spectro-polarimetry

R. Brivio<sup>1,2</sup>, S. Covino<sup>2</sup>, P. D’Avanzo<sup>2</sup>, K. Wiersema<sup>3</sup>, J. R. Maund<sup>4</sup>, M. G. Bernardini<sup>2</sup>,  
S. Campana<sup>2</sup>, and A. Melandri<sup>2</sup>

<sup>1</sup> Università degli Studi dell’Insubria, Dipartimento di Scienza e Alta Tecnologia, via Valleggio 11, 22100 Como, Italy

<sup>2</sup> INAF–Osservatorio Astronomico di Brera, via E. Bianchi 46, 23807 Merate (LC), Italy

e-mail: [riccardo.brivio@inaf.it](mailto:riccardo.brivio@inaf.it)

<sup>3</sup> Physics Department, Lancaster University, Lancaster LA1 4YB, UK

<sup>4</sup> Department of Physics and Astronomy, University of Sheffield, Hicks Building, Hounsfield Road, Sheffield S3 7RH, UK

Received 14 April 2022 / Accepted 26 August 2022

## ABSTRACT

**Context.** Among the large variety of astrophysical sources that we can observe, gamma-ray bursts (GRBs) are the most energetic of the whole Universe. Their emission peaks in the  $\gamma$ -ray band, with a duration from a fraction of a second to a few hundred seconds, and is followed by an afterglow covering the whole electromagnetic spectrum. The definition of a general picture describing the physics behind GRBs has always been a compelling task, but the results obtained so far from observations have revealed a puzzling landscape. The lack of a clear, unique paradigm calls for further observations and additional, independent techniques for this purpose. Polarimetry constitutes a very useful example as it allows us to investigate some features of the source such as the geometry of the emitting region and the magnetic field configuration.

**Aims.** To date, only a handful of bursts detected by space telescopes have been accompanied by ground-based spectro-polarimetric follow-up, and therefore such an analysis of more GRBs is of crucial importance in order to increase the sample of bursts with multi-epoch polarisation analysis. In this work, we present the analysis of the GRB 080928 optical afterglow, with observations performed with the ESO-VLT FORS1 instrument.

**Methods.** Starting from raw data taken in the imaging polarimetry (IPOL) and spectro-polarimetry (PMOS) modes, we performed data reduction, followed by the photometric analysis of IPOL data, taken  $\sim 14$  and  $\sim 40$  h after the burst detection, and spectroscopy of PMOS data ( $t \sim 14.95$  h). After computing the reduced Stokes parameters  $Q/I$  and  $U/I$ , which describe the linear polarisation of the emitted radiation, we obtained the polarisation degree for the three observing epochs.

**Results.** We find that the GRB optical afterglow was not significantly polarised on the first observing night. The polarisation degree ( $P$ ) grew on the following night to a level of  $P \sim 4.5\%$ , giving evidence of polarised radiation at a  $4\sigma$  confidence level. The GRB 080928 light curve is not fully consistent with standard afterglow models, making any comparison with polarimetric models partly inconclusive. The most conservative interpretation is that the GRB emission was characterised by a homogeneous jet and was observed at an angle of  $0.6 < \theta_{\text{obs}}/\theta_{\text{jet}} < 0.8$ . Moreover, the non-zero polarisation degree on the second night suggests the presence of a dominant locally ordered magnetic field in the emitting region.

**Key words.** gamma-ray burst: individual: GRB 080928 – polarization

## 1. Introduction

Gamma-ray bursts (GRBs) represent the brightest events we can observe in the Universe, reaching  $10^{54}$  erg  $s^{-1}$  of isotropic equivalent energy. They are made up of a bright, prompt phase peaking in the  $\gamma$ -ray band, and a long-lasting (from hours to days or even weeks and months), fading afterglow that covers the electromagnetic spectrum at all wavelengths (Mészáros & Rees 1997; Sari et al. 1998; Piran 1999). The observation of the prompt phase duration of several bursts revealed a bimodal distribution (Kouveliotou et al. 1993) that led to a classification into two categories: long (LGRBs) and short (SGRBs), with the separation at about 2 s. These phenomena are the result of the collapse of a massive star or the merger of compact binaries, with a significant fraction of the long GRBs associated with core-collapse supernovae (see Cano et al. 2017, for a review). Accretion onto the resulting compact object (either a black hole or a neutron star) produces powerful ultra-relativistic jets generating the prompt emission through dissipation processes like shocks or magnetic reconnection (for a review of GRB physics, see e.g. Zhang & Mészáros 2004; Gehrels et al. 2009; Kumar & Zhang

2015). The afterglow is instead produced when the resulting rapidly expanding ejecta of a GRB collide with the surrounding medium. As the collision-driven afterglow emerges, shocks are formed: one forward-propagating into the external medium and another shorter-lived reverse shock propagating backward into the jet (Sari & Piran 1999; Kobayashi 2000). The relative importance of these shocks is set by some micro-physical parameters, depending on the magnetic field and electron energies.

At present, a large number of GRBs have been observed, especially after the launch of dedicated missions like the Neil Gehrels Swift Observatory (hereafter *Swift*, Gehrels et al. 2004) in 2004 and *Fermi* Gamma-Ray Space Telescope, with its Large Area Telescope (LAT, Atwood et al. 2009) and Gamma-ray Burst Monitor (GBM, Meegan et al. 2009) in 2008. Despite the effort in this field, a unique and general model reconciling all observations and inferred features of detected bursts has proven elusive. Polarimetry can allow us to prove that the fireball is beamed, to constrain the orientation of the jet with respect to the line of sight, and possibly to determine the jet geometry as well as the configuration of the magnetic fields dominating in the emitting region (for a review, see Covino & Gotz 2016). Some degree of

polarisation is expected to emerge in the optical flux of GRBs as a signature of synchrotron radiation (Mészáros & Rees 1997), and the first successful polarisation measurement was achieved for the optical afterglow (OA) of GRB 990510 (Covino et al. 1999; Wijers et al. 1999). As a general rule, some degree of asymmetry in the expanding fireball is necessary to produce some degree of polarised flux. Gruzinov & Waxman (1999) argued that if the magnetic field is globally random but with a large number of patches where the magnetic field is instead coherent, a polarisation degree of up to  $\sim 10\%$  is expected, especially at early times. High levels of polarisation in the early afterglow were observed for some GRBs, such as GRB 090102, GRB 091208, and GRB 120308A (see respectively, Steele et al. 2009; Uehara et al. 2012; Mundell et al. 2013). Ghisellini & Lazzati (1999) and, independently, Sari (1999), considered a geometrical setup in which a beamed fireball is observed slightly off-axis. This break of symmetry again results in a significant polarisation degree. Their model also predicts a testable variation of the polarisation degree and position angle associated with the evolution of the afterglow light curve.

A relatively poorly explored polarimetric probe of afterglow physics is spectro-polarimetry, which extends the available polarisation measurements to a wide range of wavelengths. Multi-wavelength, simultaneous detection of polarised flux offers an additional and efficient way to explore the afterglow physics both at early and late times and from both the forward and the reverse shock. Spectro-polarimetry adds some diagnostic power especially at optical wavelengths, in particular if any of the synchrotron break frequencies (e.g. the synchrotron cooling frequency) lie within the optical band. Spectro-polarimetry is also crucial to quantify the polarisation induced by aligned dust along the line of sight in the GRB host galaxy and in our own galaxy. Indeed, it is now well-established that the optical afterglow radiation is mainly produced via synchrotron emission, whose associated polarisation is expected to be wavelength independent, while dust-induced polarisation makes the afterglow polarisation  $\lambda$ -dependent. Therefore, spectro-polarimetry is the best technique to quantify this contribution, which is likely to play a non-negligible role in the polarisation distribution of afterglows and their physical interpretation. To date, only a few afterglows have been observed with spectro-polarimetry; for example, GRB 020813 (Barth et al. 2003), GRB 021004 (Wang et al. 2003), GRB 030329 (Greiner et al. 2004), and GRB 191221B (Buckley et al. 2021).

A crucial parameter for a more complete physical interpretation of the event is the jet break time, that is, the time at which we observe an achromatic break in the afterglow light curve. Despite not being trivial, in some cases, a polarisation detection before and after the jet break was achieved, leading to a more precise modelisation of the afterglow: a decreasing polarisation from  $P = 2.26\%$  to  $P = 1.18\%$  was identified in the GRB 020813 optical afterglow (Barth et al. 2003; Gorosabel et al. 2004; Lazzati et al. 2004), while an upper limit was given from a detection almost coincident with the jet break for GRB 071010A (Covino et al. 2008); polarisation measurements before and after the jet break were also achieved for GRB 091018 (Wiersema et al. 2012) and GRB 121024A (Wiersema et al. 2014).

In this work, we analyse imaging polarimetry and spectro-polarimetry data of the optical afterglow of GRB 080928, an event that has not yet been properly analysed and published<sup>2</sup>. In Sect. 2 we report information about GRB 080928, and in Sect. 3,

the observations and data analysis procedure are described. In Sect. 4, a full discussion is presented, while our main conclusions are summarised in Sect. 5.

## 2. GRB 080928

GRB 080928 was first detected by the Burst Alert Telescope (BAT, Barthelmy et al. 2005) on board *Swift* at  $t_0 = 15:01:32.86$  UT on 2008 September 28 (Sakamoto et al. 2008). Its prompt phase lasted 112 s, making it a candidate for the Long GRB class. The main burst emission also triggered the Gamma-Ray Burst Monitor on board *Fermi* (Paciesas et al. 2008), while the INTEGRAL satellite was passing through the South Atlantic Anomaly (SAA) during the time of GRB 080928 and therefore could not observe the burst. *Swift* slew to point towards the emitting region with its X-Ray Telescope (XRT, Burrows et al. 2005) 170 s after the BAT trigger, observing until 2.7 days after the burst detection. The optical counterpart was identified by the UV/Optical Telescope (UVOT, Roming et al. 2005) from 3 min after the trigger and was located at the coordinates (J2000) RA = 6 h 20 min 16.83 s, Dec =  $-55^\circ 11' 58''.9$ , with an uncertainty of  $0.5''$ , and its redshift was found to be  $z = 1.6919$  (Fynbo et al. 2009). The prompt emission was characterised by a precursor started at  $t_0 - 90$  s and some peaks of variable intensity: the main GRB emission started at  $t_0 + 170$  s, with two peaks at 204 and 215 s. *Swift* also detected a third, fainter peak at 310 s, and stopped the observations at  $t_0 + 400$  s. The *Fermi*/GBM light curve shows only a single pulse corresponding to the main peak detected by *Swift* ( $t_{0,\text{GBM}} = t_0 + 204$  s). The optical emission was studied in detail by Rossi et al. (2011), where the X-rays and optical light curves were published. The fluence in the prompt phase in 15–150 keV band (that of *Swift*/BAT) is  $(2.1 \pm 0.1) \times 10^{-6}$  erg cm $^{-2}$ , while the 1-s peak photon flux, measured in the same band, is  $2.1 \pm 0.1$  photons cm $^{-2}$  s $^{-1}$  (errors at 90% confidence level).

Ground-based follow-up observations were performed by the ROTSE-IIIa 0.45 m telescope in Australia (Rykoﬀ et al. 2008), the Watcher telescope in South Africa (Ferrero et al. 2008), the MPG/ESO 2.2 m telescope on La Silla, Chile, equipped with the multichannel imager GROND (Rossi et al. 2008), and ESO-VLT at the Paranal Observatory, Chile (Vreeswijk et al. 2008).

## 3. Observations and data analysis

Observations of GRB 080928 were obtained by ESO VLT-UT2 (Kueyen), which is equipped with the Focal Reducer/low dispersion Spectrometer (FORIS1) with the V\_HIGH filter<sup>1</sup> ( $\lambda_0 = 5610$  Å,  $FWHM = 1230$  Å) in the imaging polarimetry mode; the 300V grism (with order sorting filter GG375) and a  $1.5''$  slit width were adopted in the spectro-polarimetry mode, with a spectrum covering the range from 3800 Å to 7600 Å. Observations were all obtained with the E2V blue-optimised CCD mounted on the instrument, and the  $2 \times 2$  binning readout mode of the CCD was adopted. All raw data, including both target observations and calibration data, were downloaded from the ESO raw data archive<sup>2</sup>. The burst is of particular interest because both optical and X-ray emissions were detected when the GRB was still radiating in the gamma-ray band. This makes it one of the rare cases (e.g. GRBs 041219A, 050820A, 051111, 061121;

<sup>1</sup> ESO filter number +114, for transmission curves see <https://www.eso.org/sci/facilities/paranal/instruments/fors1/inst/Filter/curves.html>

<sup>2</sup> <http://archive.eso.org/cms.html>

Shen & Zhang 2009) where a broad-band spectral energy distribution (SED) from about 1 eV to 150 keV can be constructed for the prompt emission phase.

Our dataset includes two observing runs with the imaging polarimetry (IPOL) mode divided into two nights: these started  $\sim 14$  h after the GRB trigger on 2008 September 28 night, and the same setup was repeated three times on the following night from  $t - t_0 \sim 40$  h. The whole IPOL dataset is reported in Table A.1. In addition, one observation in the spectro-polarimetry (PMOS) mode was performed from  $t - t_0 \sim 14.95$  h (see Table A.2). All the observing blocks reported in Table A.1 are made up of two subsets, each containing four exposures at four different angles ( $0^\circ$ ,  $22.5^\circ$ ,  $45^\circ$ ,  $67.5^\circ$ ) of the half-wave plate in the instrumental setting of FORS1. Imaging polarimetry is achieved by the use of a Wollaston prism splitting the image of each object in the field into the two orthogonal polarisation components appearing in adjacent areas of the image. A strip mask is used in the focal area of the instrument to avoid overlapping of the two beams of polarised light on the CCD. In this way, for each position angle  $\phi/2$  of the half-wave plate rotator, we obtain two simultaneous images of cross-polarisation at angles  $\phi$  and  $\phi+90^\circ$ . The dataset also includes some standard stars to be analysed: two polarised, Vela1 95 (observed in both modes) and NGC-2024 (in IPOL mode), in order to fix the offset between the polarisation and the instrumental angles, and one unpolarised, WD-2149+021 (in PMOS mode), to check for possible spurious instrumental contributions to the total polarisation degree.

Data analyses were performed for all observations by means of specific software depending on the data type. The reduction was carried out with the ESO-Eclipse package (version 5.0.0, Devillard 1997) for IPOL images and with the ESO-Reflex pipeline in PMOS mode (version 2.11.3, Freudling et al. 2013) for spectro-polarimetric data. For both of them, after bias subtraction, non-uniformities were corrected using flat-fields obtained without the Wollaston prism (see e.g. Patat & Romaniello 2006).

The flux of each point source in the field of view of IPOL data was derived by means of aperture photometry by the Graphical Astronomy and Image Analysis (*Gaia*) tools (Currie et al. 2014), with apertures chosen so as to be at least a few times the seeing. The background was estimated with annuli of radii from two to three times the seeing and applying a sigma clipping of the counts computed inside. Each pair of simultaneous measurements at orthogonal angles was used to compute the  $Q$ ,  $U$  Stokes parameters. This technique removes any difference between the two optical paths (ordinary and extraordinary ray). Moreover, being based on relative photometry in simultaneous images, our measurements are insensitive to intrinsic variations in the optical transient flux. In addition to the OA, some bright, nearby field stars were studied in order to look for possible spurious contribution, because stars are typically unpolarised sources, except for some polarisation induced by dust either in the host galaxy or in the Milky Way. All the field stars we studied are less than  $1'$  from the position of the optical afterglow, meaning that the instrumental polarisation depending on the distance from the optical axis of the instrument can be neglected (Patat & Romaniello 2006).

For the spectro-polarimetric data, 1D spectra were extracted from reduced 2D images through ESO-Midas<sup>3</sup> (version 19FEB) after checking the width of the signal by fitting the spatial profile with a Gaussian distribution. This allowed us to also compute the corresponding seeing; the values are reported in Table A.2. We then rebinned the extracted spectra so as to obtain a larger signal-to-noise ratio (S/N) in each bin: we chose a total of 50 bins from

**Table 1.** ESO-VLT FORS1 optical afterglow magnitudes.

$t - t_0$ (h)	$V$ magnitude	$\sigma_{V_{\text{mag}}}$
13.93	20.89	0.03
13.97	20.85	0.03
14.85	21.07	0.09
15.73	21.03	0.09
39.30	22.71	0.11
40.30	22.77	0.13
41.20	22.65	0.11

**Notes.**  $V$ -band magnitudes for the optical afterglow computed from the acquisition images taken before polarimetry epochs and calibrated using APASS standard stars, as described in the text.

3801.65 to 7596.65 Å, giving a spectral dispersion of 75.96 Å per bin.

The reduced Stokes parameters  $Q/I$  and  $U/I$  describing the linear polarisation of the radiation were derived using the following formulae:

$$\frac{Q}{I} = \frac{1}{2} \left( \frac{f_o - f_e}{f_o + f_e} \Big|_{0^\circ} - \frac{f_o - f_e}{f_o + f_e} \Big|_{45^\circ} \right)$$

$$\frac{U}{I} = \frac{1}{2} \left( \frac{f_o - f_e}{f_o + f_e} \Big|_{22.5^\circ} - \frac{f_o - f_e}{f_o + f_e} \Big|_{67.5^\circ} \right) \quad (1)$$

which make use of all data obtained at the four angles of the retarder plate. The subscripts  $_o$  and  $_e$  represent the ordinary and extraordinary rays in which the incoming radiation is split, respectively. We computed the reduced Stokes parameters from the average of the results obtained for all observing runs on the same night, and so obtained two final values for imaging polarimetry data, one per night, and one result in the spectro-polarimetry mode. Errors on the reduced Stokes parameters are computed via standard propagation theory.

In addition, we computed the magnitude of the OA corresponding to the polarimetry epochs: before each observing run, acquisition images of the sky were obtained, from which we could derive magnitudes in  $V$ -band. The data were calibrated using field stars from the AAVSO Photometric All-Sky Survey Data Release 9 (APASS DR9, Henden et al. 2016): we made use of some field stars, whose FORS  $V$ -band magnitudes were compared with  $V$  magnitudes from APASS. In this way, we found the appropriate correction to be applied to the afterglow magnitude by fine-tuning the zero-point on each acquisition image. The results obtained for the optical transient are shown in Table 1, and were added to the whole data set of optical and near-infrared observations for GRB 080928 afterglow, including the ground-based follow-up and the *Swift*/UVOT observations. Data were taken from Tables A.1, A.2, and A.3 in Rossi et al. (2011). The complete set is plotted in Fig. 1; moreover, for the sake of clarity regarding the afterglow time evolution, we show  $R$ -band and  $J$ -band data only in Fig. 2: after an initial, almost constant behaviour, the flux undergoes a power law-like decrease from  $t - t_0 \sim 10^{-1}$  days.

## 4. Results

After computing and averaging the Stokes parameters, we obtained (for IPOL data) the  $Q/I$ ,  $U/I$  plots reported in Figs. 3 and 4. They include the OA and the field stars, with bars representing  $1\sigma$  errors. All the field stars are isolated, unsaturated

<sup>3</sup> <https://www.eso.org/sci/software/esomidas/>

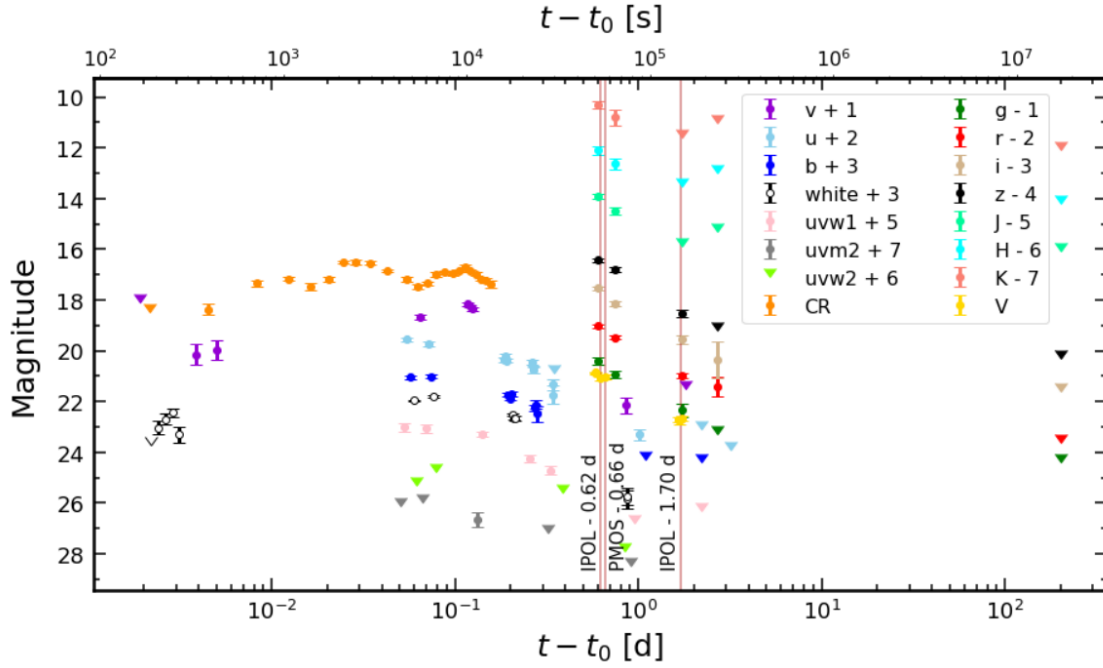


**Fig. 1.** Complete photometric optical/NIR data set of the afterglow of GRB 080928 from *Swift*/UVOT (all but the last filter in the first column of the legend), ROTSE-IIIa (CR, i.e. unfiltered *R*-equivalent Vega magnitudes), GROND (all but the last filter in the second column of the legend), and VLT-FORS (*V* filter) observations. All magnitudes are given in the Vega system, with colours shifted by the values given in the legend for clarity. Downward pointing triangles indicate upper limits; *uvw2* was the only filter in which only upper limits could be derived. The vertical lines mark the time of our polarimetric measurements.

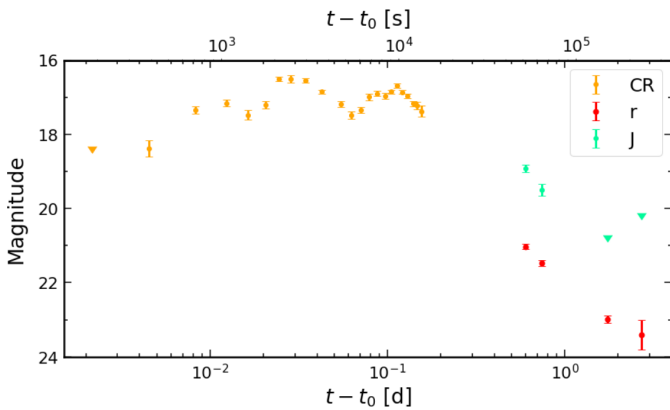


**Fig. 2.** *R*-band and *J*-band points from the complete data set shown in Fig. 1, without shift in magnitude, to show the temporal evolution of the optical-NIR afterglow of GRB 080928. Optical *r*-band flux is nearly constant up to  $t - t_0 \sim 10^{-1}$  days, before it decreases as expected for standard afterglows; NIR *J*-band observations show a similar decrease even if two points and only two upper limits were obtained.

in every epoch and at least comparable in brightness to the afterglow in the first epoch. During the first night, we notice that the location of the optical afterglow does not differ significantly from the locations of the fields stars, and therefore we do not have evidence of polarised radiation emitted  $\sim 14$  h after the burst. On the second night, instead, the OA is far from the cluster of field stars on the  $Q/I, U/I$  plot, providing possible evidence of polarised radiation. As for the spectra, we summed all results obtained in PMOS mode and obtained the spectra reported in Fig. 5. To compute the polarisation degree, we considered only the range in wavelength corresponding to the one of the V\_HIGH filter used for IPOL observations, so as to make a comparison.

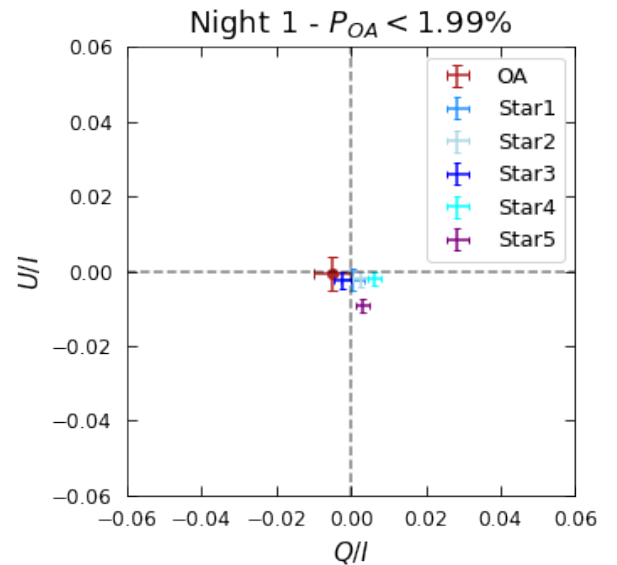


**Fig. 3.**  $Q/I, U/I$  plot from the IPOL observation on the night of 2008 September 28. The position of the optical afterglow (red bars) does not differ markedly from the other points, which represent some bright field stars observed near the transient and expected to be unpolarised. Therefore, the polarisation of the OA is consistent with zero, and only a  $3\sigma$  upper limit is given (see value above the plot).

From the analysis of the standard stars observed in the imaging polarimetry mode, we derived a polarisation angle for Velal 95 of  $\theta_{\text{Vela}} = 172.33 \pm 0.27$ , while the expected one is  $\theta_{\text{exp, Vela}} = 172.1 \pm 0.1^4$ ; by applying the same analysis to NGC-2024 we found  $\theta_{\text{NGC}} = 136.55 \pm 0.26$ , with an expected

<sup>4</sup> <https://www.eso.org/sci/facilities/paranal/instruments/fors/inst/pola.html>

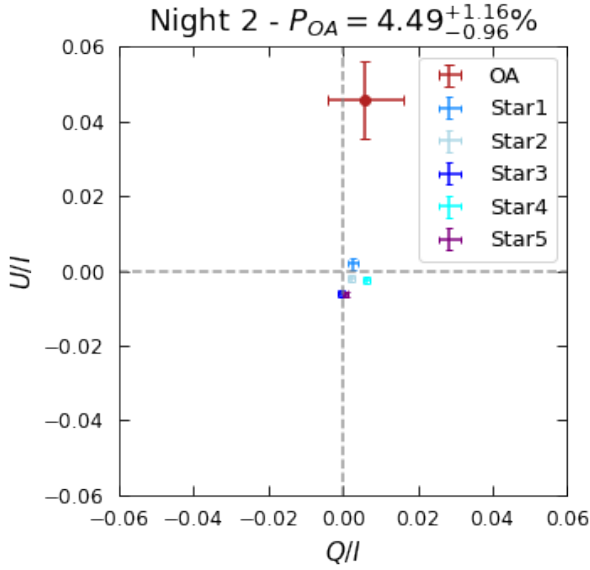


**Fig. 4.**  $Q/I, U/I$  plot from IPOL observation on the night of 2008 September 29. The position of the optical afterglow (red bars) is now far away from the cluster formed by the field stars, which are still expected to be unpolarised. For this reason, at a confidence level slightly larger than  $4\sigma$  (see values above the plot), we can state that the optical transient is polarised.

value of  $\theta_{\text{exp,NGC}} = 135.94 \pm 0.2$  (Cikota et al. 2017). Therefore, the analysis of polarimetric standard stars revealed consistency with expected values within  $1\sigma$  for Vel 195 and  $1.5\sigma$  for NGC 2024. Moreover, the average polarisation of the field stars is consistent with zero: on the first night, we obtained  $\langle Q/I \rangle = 0.0025 \pm 0.0027$ ,  $\langle U/I \rangle = 0.0016 \pm 0.0012$ , while on the second night we derived  $\langle Q/I \rangle = 0.0017 \pm 0.0016$ ,  $\langle U/I \rangle = 0.0011 \pm 0.0004$ . The degree  $P$  and angle  $\theta$  of polarisation are obtained from the measurements of  $Q/I$  and  $U/I$  for the OA [ $P = \sqrt{Q^2 + U^2}/I$ ,  $\theta = \frac{1}{2} \arctan(U/Q)$ ] after correcting for the polarisation induced by the instrument or by the local interstellar matter ( $\langle Q/I \rangle$ ,  $\langle U/I \rangle$ ). Moreover, for any low level of polarisation, ( $P/\sigma_P \leq 4$ ), the distribution function of  $P$  and of  $\theta$  is no longer normal and that of  $P$  becomes skewed. A correction taking into account this bias is required, and we adopted the modified asymptotic estimator defined by Plaszczyński et al. (2014) to derive the correct value of the polarisation degree  $P$ . In this way, we obtained the final results for the polarisation of the OA and report them in Table 2. As we found very low values of  $P/\sigma_P$  for the observations taken on the first night, we report only  $3\sigma$  upper limits for the polarisation degree  $P$ , while an evaluation of the position angle evolution was not possible. We notice that there is no significant polarisation on the first night, as confirmed also from PMOS results, while we found polarisation on the following night at more than  $4\sigma$  confidence level (CL). We also combined the results obtained on the first night in both IPOL and PMOS mode to obtain an average value for the polarisation detected on 2008 September 28, yielding a  $3\sigma$  upper limit of  $P < 1.06\%$ . The evolution of the polarisation with time is shown in Fig. 6. The polarisation is consistent with zero on the first night, as already pointed out, and it increases towards the value obtained for the second night. No further observations were available to follow the later evolution of the polarisation curve.

As already pointed out in Sect. 1, the dust present in both the GRB host galaxy and the Milky Way (MW) can contribute

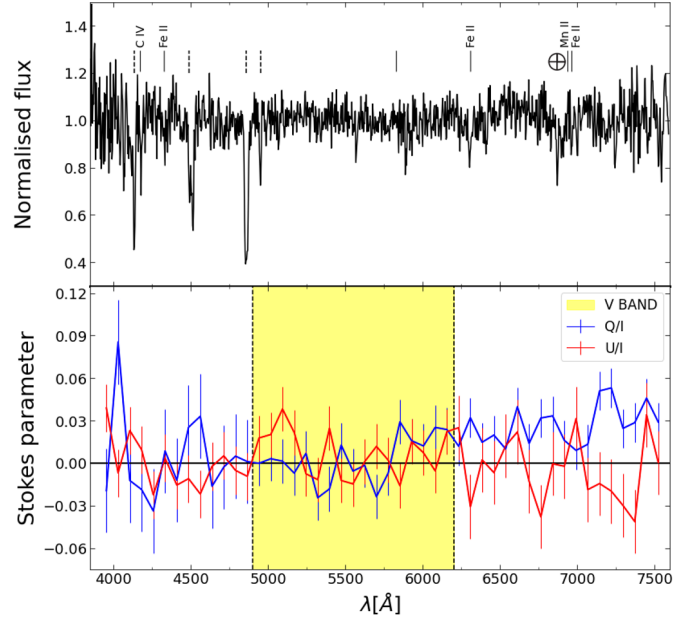


**Fig. 5.** Results of GRB 080928 spectroscopic analysis.

*Top:* GRB 080928 normalised spectrum obtained from FORS1/PMOS data taken from  $t \sim 14.95$  h after the burst on 2008 September 28. Spectral lines from GRB 080928 absorption system at  $z = 1.6919$  are marked with vertical solid lines, while the ones from an intervening system at  $z = 0.7359$  are represented by vertical dashed lines (for details, see Fynbo et al. 2009). *Bottom:*  $Q/I, U/I$  Stokes parameters spectra derived from FORS1/PMOS data. The highlighted yellow region corresponds to the V-band in which IPOL data were taken in order to perform a consistent comparison between data taken with the two observing modes. The spectra have been rebinned as described in the text.

to the total polarisation degree. Starting from the host extinction estimated by Rossi et al. (2011), we tried to put some limits on the polarisation contribution from the dust in the host galaxy: different dust recipes were considered (SMC, LMC, and MW for Small and Large Magellanic Clouds and Milky Way extinction laws, respectively; Gordon et al. 2003, 2009) in order to try to derive the local extinction  $A_V$ , which was found to be in the 0.04–0.37 mag range, depending on the specific model adopted. It is possible to put an upper limit on the contribution of the galactic interstellar polarisation:  $P_{\text{ISP}}(\%) \leq 9.0 \times E(B - V)$ . If we assume a MW-like behaviour of the dust in the host galaxy, we can derive  $E(B - V) = A_V/R_V \leq 0.12$ , where we have considered the larger estimate for  $A_V$  (0.37) and  $R_V = 3.1$ , that is, the average value for our galaxy. This yields a maximum contribution from the GRB host galaxy dust of  $P_{\text{HG}} \sim 1.1\%$ , which is significantly lower than the upper limit we derived. In order to investigate the significance of this possible contribution, we tried a fit of the polarisation spectrum in a Bayesian framework with either a Serkowski law (Serkowski et al. 1975) or the predictions in the optical band for a standard afterglow, that is, a constant value. A fit with a Serkowski law is satisfactory and gives  $\lambda_{\text{max}} \sim 0.8 \mu\text{m}$ , likely driven by the apparent polarisation increase in the reddest part of the spectrum (Fig. 5). A large value for  $\lambda_{\text{max}}$  is not unprecedented in young stellar population environments (e.g. Patat et al. 2015). However, a constant (afterglow) value for the polarisation also provides a good fit and the preference for the more complex model with respect to the simpler afterglow, computed by their respective Bayes factors, is only at  $\sim 2.4\sigma$ , preventing us from deriving further conclusions.

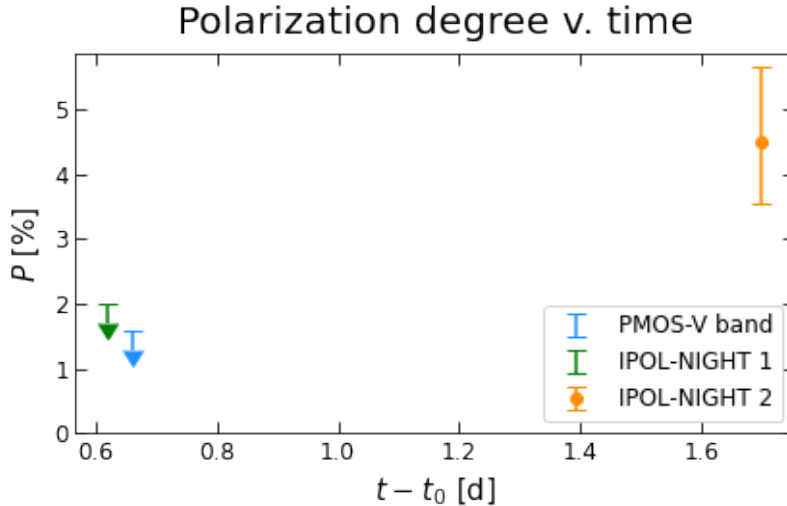


**Fig. 6.** Evolution of the polarisation degree  $P$  of GRB 080928, both in imaging polarimetry and spectro-polarimetry mode. The afterglow is unpolarised at early times ( $\sim 14$ – $15$  h after the trigger), while  $P$  significantly increases about one day after (at  $t - t_0 \sim 40.7$  h). As we could only derive upper limits on the first night, we cannot properly analyse the evolution of the position angle with time.

**Table 2.** Results of GRB 080928 optical afterglow polarimetric observations.

$t - t_0$ (days)	MODE	$Q/I$	$U/I$	$P$ (%)	$\theta$ ( $^\circ$ )
0.62	IPOL	$-0.0049 \pm 0.0050$	$-0.0008 \pm 0.0045$	$<1.99$	–
0.66	PMOS	$0.0031 \pm 0.0034$	$0.0037 \pm 0.0038$	$<1.57$	–
1.70	IPOL	$0.0059 \pm 0.0101$	$0.0457 \pm 0.0104$	$4.49^{+1.16}_{-0.96}$	$41.3 \pm 6.3$

**Notes.** Summary of the results in both imaging and spectro-polarimetry mode. The latter were obtained by integrating the spectrum over the V-band. Errors on the reduced Stokes parameters and the position angle were computed via propagation theory; those on  $P$  were obtained after bias correction when appropriate (see text). Uncertainties are at  $1\sigma$ , while upper limits are at  $3\sigma$ .

## 5. Discussion

In the previous section, we discuss the possibility that the total polarisation we detect could be the combination of the intrinsically polarised radiation from the GRB optical afterglow and an additional contribution from dust in the host galaxy and/or in the Milky Way, which can be constrained by analysing the spectral dependence of the polarisation degree. The analysis of PMOS data allowed us to derive only an upper limit for  $P$ , possibly pointing to intrinsically unpolarised radiation and a negligible contribution of the dust aligned along the line of sight. In principle, this low value may also be due to the combination of a dust-induced contribution and non-zero intrinsic polarisation, which cancel out due to a phase shift of their position angle with respect to each other (e.g. Lazzati et al. 2004). However, the Serkowski fit we performed on the polarisation spectrum did not prove solid evidence of a relevant dust contribution. For this reason, we decided to adopt in the following discussion the scenario with the lowest number of parameters, and we consider the dust-induced polarisation as negligible.

The time dependence of the polarisation degree reported in Fig. 6 can be compared with the expected behaviour depending on some features of the emitting region, the jet geometry in particular. Rossi et al. (2004) studied different jet configurations, with and without the possibility of lateral expansion, and derived the corresponding expected light curves and polarisation curves. An extensive range of values for  $P$  can be obtained depending on some parameters, e.g. the observer viewing angle and the jet break time. If the observer viewing angle is lower than the jet

aperture angle, we expect a relatively low polarisation degree, from a few % to a maximum of  $\sim 25\%$  for  $\theta_{\text{obs}} = \theta_{\text{jet}}$ . For off-axis observations the larger the observing angle, the later and the stronger the polarisation peak: even  $P \sim 50\%$  can be achieved in principle, but such a large polarisation degree has never been observed. In general, the time evolution of the curves strongly depends on the jet configuration, therefore it is important to perform multi-epoch observations to properly compare the observed polarisation curve with the theoretical expectations and possibly infer the intrinsic properties of the jet and the emitting region.

These models are based on random magnetic fields that are confined to the shock, while Teboul & Shaviv (2021) also considered more complex models of the magnetic field configuration, from which they derived some polarisation predictions. In addition to the situation considered by Rossi et al. (2004), Teboul & Shaviv (2021) computed expectations for an anisotropic random field, yielding a similar behaviour, that is two peaks separated by a  $90^\circ$  position angle swing for an observer inside the jet. Then, they added to the random field an additional, ordered component (still confined to the shock) whose relative importance is set by the random-to-ordered ratio,  $\mu$ . Teboul & Shaviv (2021) observed that the polarisation peak amplitude for off-axis observers is not significantly affected by  $\mu$ , while the value away from the maximum is much more sensitive to it. They finally added an anisotropy factor to the previous expectations, yielding a significant difference in the case where  $\theta_{\text{obs}} > \theta_{\text{jet}}$ , while for an observer inside the jet, the expectations do not depend to a significant extent on the anisotropy factor. The rotation of the position angle is analysed as well: the  $90^\circ$  swing is expected for observers

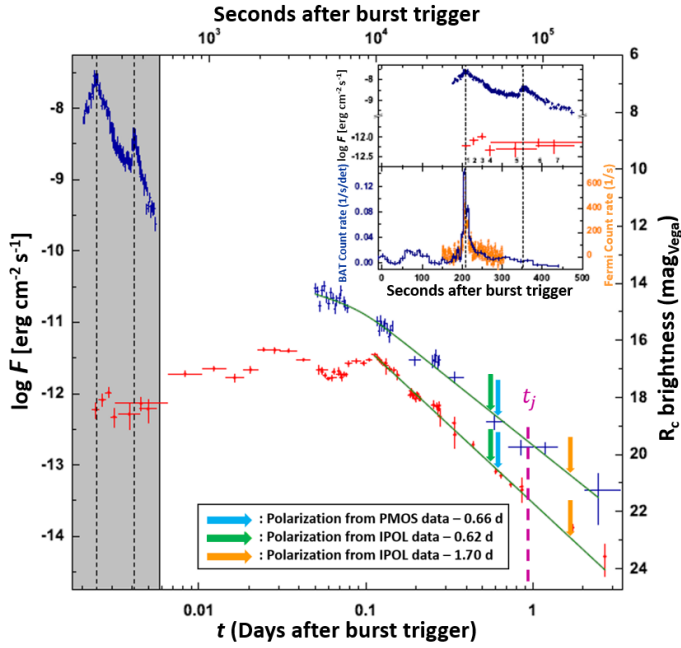


**Fig. 7.** Optical (red points) and X-ray (blue bars, in 0.3–10 keV band) light curve of GRB 080928 afterglow. The green curve is the best fit of the late-time data, while the grey-shaded region on the left shows the early phase. The latter is also represented in the inset and compared with the prompt-phase emission detected by *Fermi*-GBM and *Swift*/BAT. The arrows above the best fit curves on the right represent the epochs of polarimetric observations obtained with ESO-VLT FORS1, both in the imaging polarimetry and spectro-polarimetry mode, and the assumed jet break time  $t_j$  is indicated by the purple dashed line (Rossi et al. 2011).

inside the jet axis and only if the field is totally random, whereas the rotation is smaller if we add an ordered component. Its value depends on the direction and the intensity of the ordered field.

The light curve obtained for GRB 080928 (Fig. 4 in Rossi et al. 2011) is shown in Fig. 7, both in X-rays and optical band. We identify a power-law decay. The X-ray data can be fit after  $t = 4.2$  ks from the detection with a broken power-law with indices  $\alpha_1^X = 0.72 \pm 0.35$  and  $\alpha_2^X = 1.87 \pm 0.07$ , and a break time  $t_b^X = 0.094 \pm 0.019$  days (all errors are  $1\sigma$  uncertainties). The optical curve follows a single power-law decay with index  $\alpha^{\text{opt}} = 2.17 \pm 0.02$  after  $t = 10$  ks, while the complex behaviour observed before can be due to the prolonged activity of the central engine or to the presence of a precursor observed at  $t_0 - 90$  s (see Sect. 2). If both the precursor and the main event originate from the same central engine, we could expect a non-standard afterglow with multiple peaks (for more details, see Nappo et al. 2014). However, we can observe this evolution in the optical data only, and the lack of X-ray data from  $\sim 0.5$  ks to 3 ks prevents us from discussing this scenario in more detail.

The interpretation of the results and the comparison with expected models strongly depend on the jet break time  $t_j$ , which is expected to occur at different times depending on the viewing angle of the observer, the geometry of the jet, and the potential sideways expansion. According to the most popular afterglow models, the jet break time is achromatic, and therefore we should have  $t_j^X = t_j^{\text{opt}}$ , and we expect the X-ray and optical light curves to have the same decay index after the jet break. GRB 080928 light curves are not consistent with this behaviour because  $\alpha_2^X \neq \alpha^{\text{opt}}$ . Moreover, we were not able to identify a break at  $t_b^X$  in the

optical curve due to its peculiar evolution. Even if a different index decay after the jet break is not an unprecedented behaviour (see Kann et al. 2010; Zaninoni et al. 2013; Melandri et al. 2014), according to Leventis et al. (2014) the break pointed out in the X-ray curve at  $t_b^X$  is likely to be interpreted as an injection break. Leventis et al. (2014) also assume the jet break to occur at  $t_j = 80$  ks = 0.93 days, which is in between our polarimetry epochs, as shown by the arrows and the dashed line in Fig. 7.

By comparing our light curve and polarisation curve with the expected ones from different jet geometries presented in Rossi et al. (2004), we can identify the range of values expected for  $P$ . In the case of a homogeneous jet, we expect two maxima in the polarisation curve (the second always larger than the first), with a period of null polarisation and  $90^\circ$  rotation of the position angle in between. Depending on the parameter for the jet configuration, at some viewing angle this time should coincide with the jet break time, and slightly later or before at different  $\theta_{\text{obs}}$ . If the burst is observed at an angle  $\theta_{\text{obs}} < \theta_{\text{jet}}$ , the maxima of the curve can vary from  $P \sim 2\%$  to  $P \sim 20\%$ , depending on the observer’s viewing angle and the presence of a sideways expanding (SE) or a non-sideways expanding (NSE) jet. In particular, we see that the larger  $\theta_{\text{obs}}/\theta_{\text{jet}}$ , the earlier the jet break (and the period of null polarisation) is expected to occur. If  $t_j = 0.93$  days is the actual jet break, we expect to have  $P$  close to zero at  $t \sim t_j$  for  $0.6 \leq \theta_{\text{obs}}/\theta_{\text{jet}} \leq 0.8$ . The polarisation degree on the first night would be in the  $\sim 1\text{--}4\%$  range, while on the second night it would range from  $\sim 4\%$  to a maximum value of  $\sim 8\%$  for  $\theta_{\text{obs}}/\theta_{\text{jet}} = 0.8$ . These values are derived from the NSE-jet model, whereas for a SE jet the expected values are slightly smaller (by  $\sim 1\%$ ). Alternatively, in the case of a structured or Gaussian jet, we expect similar non-zero polarisation before and after the jet break, which is at odds with our results. Only additional observations at earlier time might have allowed us a better comparison with the expectations from these jet configurations. A proper modelling is also difficult here because the polarisation curves depend on the opening angle of the jet core, a parameter that we cannot constrain for GRB 080928. We can conclude that the expected values for  $P$  for a homogeneous jet are consistent with our results: both the upper limits for the first night and the detection on the second night are within the low end of the range of expected values. The detection would be placed on the second rise of the polarisation curve. Therefore, we can state that we probably observed a homogeneous jet close to the jet axis, but we do not have enough data to discriminate between a NSE and a SE jet. Earlier observations would have provided additional data to look for a polarisation different from zero before  $t_j$  (i.e. possibly coincident with the first peak) and a potential  $90^\circ$  swing of the position angle, as observed in GRB 091018 (Wiersema et al. 2012) and GRB 121024 (Wiersema et al. 2014). Unfortunately, no data were taken before  $t - t_0 \sim 0.62$  days.

Comparison with models derived by Teboul & Shaviv (2021) cannot yield quantitative results because we would need a large number of parameters that we cannot constrain for this source, making it impossible to distinguish between any of the proposed configurations. We also compared our results with the sample of afterglows with both a jet break and a polarisation detection presented by Stringer & Lazzati (2020): GRB 080928 shows a larger polarisation degree than the average, but it is still consistent with the sample within the uncertainties.

Therefore, as mentioned above, our results are consistent with the scenario of a homogeneous jet, while only a larger dataset would have allowed us to make a comparison with the predictions from more complex jet structures. In addition to

that, from the comparison with the expected polarisation curves computed by Rossi et al. (2004) and Teboul & Shaviv (2021), we derived that the presence of significantly polarised radiation on the second night suggests that the emitting region was likely characterised by some degree of locally ordered magnetic fields. Indeed, we can generally identify locally ordered fields when we have a non-zero polarisation degree (Granot & Königl 2003), while a null value is probably associated with a random magnetic field configuration, although our sparse dataset does not allow us to draw more quantitative conclusions.

## 6. Conclusions

We present multi-epoch observations and a polarisation study of the optical afterglow of GRB 080928, which was first detected by *Swift* and *Fermi* telescopes. The ground-based polarimetric follow-up performed by means of the ESO-VLT FORS1 instrument allowed us to perform a polarimetric analysis of the source in both imaging and spectro-polarimetry modes, a significant result in itself because, from a total of more than 1500 GRBs observed by *Swift* to date, IPOL data were only collected for about 20 of them, and PMOS data were collected for only four (those cited in Sect. 1). This kind of measurement was made possible by the brightness of the event, which allowed us to collect data up to a couple of days after the trigger of the GRB. Thanks to polarimetry, we can investigate additional features of the emitting region and try to constrain, for example, the jet aperture angle and the local magnetic field configuration.

In the specific case of GRB 080928, the modelling was not fully satisfactory; for example, the afterglow light curves do not follow the standard afterglow models. The analysis performed in this work led to the addition of another source in the limited sample of GRBs studied using the polarimetry technique: we have evidence of polarised radiation after  $\sim 1.7$  days from the initial detection at a  $4\sigma$  CL, with the polarisation curve rising towards this value from the non-polarised radiation detected on the first night. Detailed spectral modelling did not allow us to single out the possible contributions from the dust aligned along the line of sight and the intrinsic polarisation of the OA to the total polarisation degree. Indeed, the fit of the polarisation spectrum could be consistent with both a pure afterglow model and a Serkowski-like behaviour (see Sect. 4). This result, together with the fact that we observe a significant variation for  $P$ , suggests that the observed polarisation is largely intrinsic. Moreover, if the jet break is fixed at  $t_j = 0.93$  days, we may conclude that we observed a homogeneous jet slightly off-axis, with  $0.6 \leq \theta_{\text{obs}}/\theta_{\text{jet}} \leq 0.8$ . The lack of both earlier and later time measurements prevents us from deriving additional conclusions linked to the behaviour of the position angle and to the further evolution of both the light curve and the polarisation curve, which could in principle reveal more information about the source. Moreover, the availability of X-ray data between 0.5 ks and 3 ks would have allowed us to compare the observations with the theoretical X-ray curves expected from the high-latitude emission (HLE) from a structured jet seen off-axis. Indeed, by constraining the viewing angle of the observer from polarisation measurements, we could in principle test the theoretical models developed to possibly explain the plateau often observed in the X-ray light curves of GRBs (see Ascenzi et al. 2020). This could be an interesting comparison for the future detection of polarised radiation from GRBs.

To date, polarisation measurements have been obtained with a rather irregular and, in some cases, limited temporal sampling. Complete coverage of both the light curve and the

polarisation curve would permit a complete analysis. In particular, the opportunity to observe polarisation from very bright GRBs before and after the jet break from more bursts would allow us to compare them to the theoretical models in a very detailed way. Long-time polarisation observations with ground-based telescopes are a very demanding task, because they require a lot of observation time, but would be worthwhile given the progress that could be made in the field of GRB physics as a result. In particular, multi-epoch spectro-polarimetric observations could help to single out contributions from the host galaxy and the Milky Way, resulting in a refined measurement of the GRB intrinsic polarisation degree  $P$  and could allow analysis of the polarisation properties of the dust in distant galaxies, a poorly studied feature in such systems. In addition, more precise measurements could help us to follow the evolution of both  $P$  and  $\theta$ , which may help in putting more stringent constraints on the micro-physics parameters driving the synchrotron emission; on the jet geometry (e.g. the aperture angle, the Lorentz factor  $\Gamma$ ); and on the specific configuration of local magnetic fields. Extending this kind of analysis to a large number of bursts would provide a wider sample with which to analyse and possibly realise a statistical study in the future.

We show that with multi-epoch imaging polarimetry and spectro-polarimetry analyses, it is possible to derive the intrinsic polarisation of the optical afterglow at different times and wavelengths and to study the structure of GRB outflows, which will hopefully lead to a better understanding of the physical processes that give rise to these extremely bright astrophysical sources.

*Acknowledgements.* The authors thank the referee for the very constructive comments and Gianpiero Tagliaferri for useful discussions. The present work is based on observations collected at the European Southern Observatory under ESO programme 081.D-0192. S.C., P.D.A. and A.M. acknowledge funding from the Italian Space Agency, contract ASI/INAF no. I/004/11/5. K.W. acknowledges support through a UK Research and Innovation Future Leaders Fellowship (MR/T044136/1) awarded to Dr. B. Simmons.

## References

- Ascenzi, S., Oganessian, G., Salafia, O. S., et al. 2020, *A&A*, 641, A61  
 Atwood, W. B., Abdo, A. A., Ackermann, M., et al. 2009, *ApJ*, 697, 1071  
 Barth, A. J., Sari, R., Cohen, M. H., et al. 2003, *ApJ*, 584, L47  
 Barthelmy, S. D., Barbier, L. M., Cummings, J. R., et al. 2005, *Space Sci. Rev.*, 120, 143  
 Buckley, D. A. H., Bagnulo, S., Britto, R. J., et al. 2021, *MNRAS*, 506, 4621  
 Burrows, D. N., Hill, J. E., Nousek, J. A., et al. 2005, *Space Sci. Rev.*, 120, 165  
 Cano, Z., Wang, S.-Q., Dai, Z.-G., & Wu, X.-F. 2017, *Adv. Astron.*, 2017, 8929054  
 Cikota, A., Patat, F., Cikota, S., & Faran, T. 2017, *MNRAS*, 464, 4146  
 Covino, S., & Gotz, D. 2016, *Astron. Astrophys. Trans.*, 29, 205  
 Covino, S., Lazzati, D., Ghisellini, G., et al. 1999, *A&A*, 348, L1  
 Covino, S., D'Avanzo, P., Klotz, A., et al. 2008, *MNRAS*, 388, 347  
 Currie, M. J., Berry, D. S., Jenness, T., et al. 2014, in *Astronomical Society of the Pacific Conference Series*, 485, Astronomical Data Analysis Software and Systems XXIII, eds. N. Manset, & P. Forshay, 391  
 Devillard, N. 1997, *The Messenger*, 87, 19  
 Ferrero, A., French, J., & Melady, G. 2008, *GRB Coordinates Network*, 8303, 1  
 Freudling, W., Romaniello, M., Bramich, D. M., et al. 2013, *A&A*, 559, A96  
 Fynbo, J. P. U., Jakobsson, P., Prochaska, J. X., et al. 2009, *ApJS*, 185, 526  
 Gehrels, N., Chincarini, G., Giommi, P., et al. 2004, *ApJ*, 611, 1005  
 Gehrels, N., Ramirez-Ruiz, E., & Fox, D. B. 2009, *ARA&A*, 47, 567  
 Ghisellini, G., & Lazzati, D. 1999, *MNRAS*, 309, L7  
 Gordon, K. D., Clayton, G. C., Misselt, K. A., Landolt, A. U., & Wolff, M. J. 2003, *ApJ*, 594, 279  
 Gordon, K. D., Cartledge, S., & Clayton, G. C. 2009, *ApJ*, 705, 1320  
 Gorosabel, J., Röl, E., Covino, S., et al. 2004, *A&A*, 422, 113  
 Granot, J., & Königl, A. 2003, *ApJ*, 594, L83  
 Greiner, J., Klose, S., Reinsch, K., et al. 2004, in *Gamma-Ray Bursts: 30 Years of Discovery*, eds. E. Fenimore, & M. Galassi, *American Institute of Physics Conference Series*, 727, 269  
 Gruzinov, A., & Waxman, E. 1999, *ApJ*, 511, 852



- Henden, A. A., Templeton, M., Terrell, D., et al. 2016, VizieR Online Data Catalog: [II/336](#)
- Kann, D. A., Klose, S., Zhang, B., et al. 2010, [ApJ](#), **720**, 1513
- Kobayashi, S. 2000, [ApJ](#), **545**, 807
- Kouveliotou, C., Meegan, C. A., Fishman, G. J., et al. 1993, [ApJ](#), **413**, L101
- Kumar, P., & Zhang, B. 2015, [Phys. Rep.](#), **561**, 1
- Lazzati, D., Covino, S., Gorosabel, J., et al. 2004, [A&A](#), **422**, 121
- Leventis, K., Wijers, R. A. M. J., & van der Horst, A. J. 2014, [MNRAS](#), **437**, 2448
- Meegan, C., Lichti, G., Bhat, P. N., et al. 2009, [ApJ](#), **702**, 791
- Melandri, A., Covino, S., Rogantini, D., et al. 2014, [A&A](#), **565**, A72
- Mészáros, P., & Rees, M. J. 1997, [ApJ](#), **476**, 232
- Mundell, C. G., Kopač, D., Arnold, D. M., et al. 2013, [Nature](#), **504**, 119
- Nappo, F., Ghisellini, G., Ghirlanda, G., et al. 2014, [MNRAS](#), **445**, 1625
- Paciesas, B., Briggs, M., & Preece, R. 2008, [GRB Coordinates Network](#), **8316**, 1
- Patat, F., & Romaniello, M. 2006, [PASP](#), **118**, 146
- Patat, F., Taubenberger, S., Cox, N. L. J., et al. 2015, [A&A](#), **577**, A53
- Piran, T. 1999, [Phys. Rep.](#), **314**, 575
- Plaszczynski, S., Montier, L., Levrier, F., & Tristram, M. 2014, [MNRAS](#), **439**, 4048
- Roming, P. W. A., Kennedy, T. E., Mason, K. O., et al. 2005, [Space Sci. Rev.](#), **120**, 95
- Rossi, E. M., Lazzati, D., Salmonson, J. D., & Ghisellini, G. 2004, [MNRAS](#), **354**, 86
- Rossi, A., Clemens, C., Greiner, J., et al. 2008, [GRB Coordinates Network](#), **8296**, 1
- Rossi, A., Schulze, S., Klose, S., et al. 2011, [A&A](#), **529**, A142
- Rykoff, E. S., Yuan, F., & McKay, T. A. 2008, [GRB Coordinates Network](#), **8293**, 1
- Sakamoto, T., Barthelmy, S. D., Evans, P. A., et al. 2008, [GRB Coordinates Network](#), **8292**, 1
- Sari, R. 1999, [ApJ](#), **524**, L43
- Sari, R., & Piran, T. 1999, [ApJ](#), **520**, 641
- Sari, R., Piran, T., & Narayan, R. 1998, [ApJ](#), **497**, L17
- Serkowski, K., Mathewson, D. S., & Ford, V. L. 1975, [ApJ](#), **196**, 261
- Shen, R.-F., & Zhang, B. 2009, [MNRAS](#), **398**, 1936
- Steele, I. A., Mundell, C. G., Smith, R. J., Kobayashi, S., & Guidorzi, C. 2009, [Nature](#), **462**, 767
- Stringer, E., & Lazzati, D. 2020, [ApJ](#), **892**, 131
- Teboul, O., & Shaviv, N. J. 2021, [MNRAS](#), **507**, 5340
- Uehara, T., Toma, K., Kawabata, K. S., et al. 2012, [ApJ](#), **752**, L6
- Vreeswijk, P., Malesani, D., Fynbo, J., et al. 2008, [GRB Coordinates Network](#), **8301**, 1
- Wang, L., Baade, D., Hoeflich, P., & Wheeler, J. C. 2003, arXiv e-prints [[astro-ph/0301266](#)]
- Wiersema, K., Curran, P. A., Krühler, T., et al. 2012, [MNRAS](#), **426**, 2
- Wiersema, K., Covino, S., Toma, K., et al. 2014, [Nature](#), **509**, 201
- Wijers, R. A. M. J., Vreeswijk, P. M., Galama, T. J., et al. 1999, [ApJ](#), **523**, L33
- Zaninoni, E., Bernardini, M. G., Margutti, R., Oates, S., & Chincarini, G. 2013, [A&A](#), **557**, A12
- Zhang, B., & Mészáros, P. 2004, [Int. J. Mod. Phys. A](#), **19**, 2385

## Appendix A: The dataset

Table A.1. Log of ESO-VLT FORS1 imaging polarimetry observations

TIME (UT)	$t_{\text{exp}}$ [s]	ANGLE[°]	FILTER
FIRST NIGHT - 09/29/08			
05:01:57	330	0	V_HIGH
05:08:00	330	22.5	V_HIGH
05:14:03	330	45	V_HIGH
05:20:06	330	67.5	V_HIGH
05:26:32	330	0	V_HIGH
05:32:34	330	22.5	V_HIGH
05:38:38	330	45	V_HIGH
05:44:41	330	67.5	V_HIGH
SECOND NIGHT - 09/30/08			
06:25:05	330	0	V_HIGH
06:31:08	330	22.5	V_HIGH
06:37:11	330	45	V_HIGH
06:43:14	330	67.5	V_HIGH
06:49:39	330	0	V_HIGH
06:55:42	330	22.5	V_HIGH
07:01:45	330	45	V_HIGH
07:07:48	330	67.5	V_HIGH
07:19:29	330	0	V_HIGH
07:25:32	330	22.5	V_HIGH
07:31:34	330	45	V_HIGH
07:37:37	330	67.5	V_HIGH
07:44:02	330	0	V_HIGH
07:50:05	330	22.5	V_HIGH
07:56:07	330	45	V_HIGH
08:02:10	330	67.5	V_HIGH
08:14:00	330	0	V_HIGH
08:20:02	330	22.5	V_HIGH
08:26:05	330	45	V_HIGH
08:32:09	330	67.5	V_HIGH
08:38:33	330	0	V_HIGH
08:44:36	330	22.5	V_HIGH
08:50:38	330	45	V_HIGH
08:56:40	330	67.5	V_HIGH

**Notes.** GRB 080928 optical afterglow observations taken with the imaging polarimetry (IPOL) mode at ESO-VLT FORS1, on the nights of 2008 September 28 and 2008 September 29. There are a total of eight sets, two taken on the first night after the GRB event (from ~ 14 h later) and six on the following night (from 39.39 h after the burst).

Table A.2. Log of ESO-VLT FORS1 spectro-polarimetry observations

TIME (UT-09/29)	ANGLE [°]	$t_{\text{exp}}$ [s]	SEEING ["]	AIR MASS (start/end)
05:58:22	0	300	1.5	1.85/1.81
06:04:06	22.5	300	1.5	1.81/1.77
06:09:51	45	300	1.5	1.77/1.74
06:15:36	67.5	300	1.5	1.73/1.70
06:21:43	0	300	1.4	1.67/1.67
06:27:27	22.5	300	1.5	1.67/1.64
06:33:11	45	300	1.5	1.63/1.61
06:38:55	67.5	300	1.5	1.61/1.58
06:51:49	0	300	1.4	1.55/1.52
06:57:33	22.5	300	1.5	1.52/1.50
07:03:18	45	300	1.5	1.50/1.48
07:09:03	67.5	300	1.5	1.48/1.46
07:15:11	0	300	1.5	1.45/1.44
07:20:55	22.5	300	1.4	1.43/1.42
07:26:39	45	300	1.5	1.41/1.40
07:32:24	67.5	300	1.2	1.40/1.38

**Notes.** GRB 080928 optical afterglow spectro-polarimetry (PMOS) observations taken with ESO-VLT FORS1 on the night of 2008 September 28, with seeing and air mass values. The results for the seeing lie within a 5% error range with respect to a reference value of 1.5", except for the last measurement.